*Eur*opean *J*ournal of *Chem*istry

Check for updates

Structural diversity in the solid-state architectures of *bis*(4-pyridyl)acetylene and its derivatives

Ibukun Oluwaseun Shotonwa [iD] [1],* and René Theodoor Boeré [iD] [2]

[1] *Department of Chemistry, Faculty of Science, Lagos State University, Ojo, Lagos, 102101, Nigeria*
ibukun.shotonwa@lasu.edu.ng (I.O.S)
[2] *Department of Chemistry and Biochemistry, University of Lethbridge, 4401 University Drive West, Lethbridge, Alberta, T1K3M4, Canada*
boere@uleth.ca (R.T.B.)
* *Corresponding author at: Department of Chemistry, Faculty of Science, Lagos State University, Ojo, Lagos, 102101, Nigeria.*
 e-mail: ibukun.shotonwa@lasu.edu.ng *(I.O. Shotonwa).*

RESEARCH ARTICLE

ABSTRACT

The crystals of *bis*(4-pyridyl)acetylene are orthorhombic and belong to the space group *Fddd*. Solid-state investigation using conventional and Hirshfeld analytical techniques revealed valuable data and structural diversities that explain the wide gap between established crystal reports of co-crystals and metal organic frameworks and the pure form of the title compound. Hirshfeld surface analysis in this wise has proved to be a useful tool in unravelling complex intermolecular interactions and simplifying them at the 2D and 3D levels using sub-tools such as fingerprint plots and electrostatic potential surfaces. Both techniques have shown that the $H \cdots N_{pyr}$ interactions in the title compound are shorter than those in its polymorphic counterpart by 0.2 Å. The more stable network provided by hetero-molecular interactions in co-crystals and metal complexes of *bis*(4-pyridyl)acetylene shed light on their lengthy existence compared to the less favorable homo-molecular interactions in pure molecules of *bis*(4-pyridyl)acetylene.

1. Introduction

Spacers are essential components of the structural make-up of chemical compounds [1-5] and one spacer group that has drawn considerable attention to itself is the monomeric acetylene spacer. This is in connection to its wide range of applications in areas that are chemistry-related [6-8]. A striking peculiarity of acetylene bridge(s) as inclusion units in polymers, oligomers, dendrimers and related compounds is their capability to impose linearly conformed shapes on their hosts, thus enhancing their abilities to complex with metal ions, combine with other organic ligands or with self in the solid state. The linearity of the acetylene linkages in turn conforms on their hosts an all-round rigidity as well as non-collapsible cavities [6-11]. Other than the fact that the introduction of an acetylene spacer is an effective method to mitigate steric strain between two subunits such as the pyridyl [12] or phenyl derivatives [13], it has played prominent roles as a building block in generating quite a number of fascinating crystalline frameworks. For the pyridyl subunits, the combination of these factors alongside conjugation via acetylene spacer-inclusion produces fascinating structural, optical, electronic and magnetic properties which have

applicative potentials in light-emitting diodes (LEDs) [14,15], organic field-effect transistors [16] and non-linear optics (NLOs) [16]. The goal of synthetic and coordination chemists to create structurally interesting metal-organic frameworks (MOFs) and complexes from *bis*(4-pyridyl)acetylene (IUPAC name: 1,2-di(pyridin-4-yl)ethyne, **1**), a linear and rigid spacer possessing terminal pyridine binding sites with cyclically extended π-conjugation for effective coordination to metal corner units, was borne out of their fascinating varieties of molecular features especially their porosities which have potentials in gas storage and separation, drug delivery and catalysis [17-19].

Interestingly, a thorough search for close fits to the aforementioned structural specifications produced a large number of SciFinder references while the Cambridge Structural Database (CSD) turned in a total of forty-two published structures (with available 3D views) including two recent pure polymorphs with CSD refcodes OLOTUG (**1a**) [20] and OLOTUG03 (**1b**) [21]. The structure of compound **1** reported here is a re-determination of **1b**. It is quite surprising that there was the long existence of quite a number of supramolecular-relevant structures [22-26] ranging from coordination complexes, host-guest inclusion molecules, 1D,

2D and 3D grid networks and co-crystals with a rich network of intermolecular interactions [27-36] before the recently published polymorphs of pure *bis*(4-pyridyl)acetylene. With the exclusion of structures **1a** and **1b**, about twenty-three (23) of these structures represent different species while the remaining seventeen (17) stand out as repetition of existing molecular structures within the same classification. These events lead to the current intensified interest in the crystal structure of the parent compound which came into synthetic limelight before 1980 [37]. As a follow-up, we herein report a two-step comparative conventional (Mercury) and Hirshfeld surface analyses between **1** and polymorphic **1a**. The first step investigates the notable effects caused by the disparities in their internal structural parameters and the second focuses on the large-scale geometrical similarities and differences for compound **1** and other **1**-containing counterparts.

2. Experimental

2.1. General methods

Trans-4,4'-dipyridylethylene was purchased from Sigma Aldrich and used without further purification. NMR data was obtained on a Bruker Avance II 300 MHz spectrometer.

2.2. Synthesis of compound 1

Bis-(4-pyridyl)ethylene (5.00 g, 27 mmol) was dissolved in 50.00 mL of concentrated HBr at 0 °C. 5.00 mL of bromine was added in drops while stirring was ongoing resulting immediately in an orange precipitate. After the addition of all the bromine, the reaction mixture was subjected to heat at 120 °C with mild stirring for 1 hour. It was then cooled to 0 °C and the perbrominated orange solid obtained was isolated by filtration. It is then converted to the white dibromide by treatment with 2 M NaOH. For the final dehydrobromination, a suspension of the dibromide in 20.00 mL of hot tertiary butanol is given in small quantities to a boiling solution of sodium (1.40 g, 61 mmol) in 150.00 mL of absolute tertiary butanol. This mixture is refluxed for 30 minutes and then evaporated to about 80.00 mL. Excess butanolate in the solution was destroyed by adding about 10.00 mL of water. The solvent is then evaporated under reduced pressure to give a white precipitate. The white precipitate was extracted with ether three times and the ether solution is again evaporated to dryness leaving behind an orange precipitate. Recrystallizing the crude product from heptane afforded 3.63 g (75 %) of pure compound **1**. ^{1}H NMR (300 MHz, CDCl$_3$, δ, ppm): 8.63 (d, 4H, *J* = 6 Hz, Ar-H (-N)), 7.41 (d, 4H, *J* = 6 Hz, Ar-H). M.p.: 113-116 °C (Literature melting point = 114 °C [37]) (Figure 1).
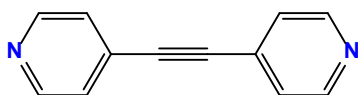
Figure 1. Molecular structure of compound **1**.

2.3. Single crystal X-ray crystallography

Selected crystal obtained via slow cooling from heptane was mounted in Paratone™ on the ends of a thin glass capillary and cooled on the goniometer head to -100 ℃ with the Bruker low-temperature accessory attached to the APEX-II diffractometer. MoKα radiation (λ = 0.71073 Å) was used for the diffraction experiment. Multi-scan absorption corrections were applied to the data sets and structures were solved using SHELX-M or SHELX-S, and refinements were conducted with full-matrix least-squares on F^2 using SHELXTL 6.14 [38]. All hydrogen atoms were located on a difference map. C-bound H

atoms were treated as riding, with C-H = 0.95 Å and U_{iso} = 1.2U_{eq} (C) for aromatic H atoms [39]. Crystal Data for C$_{12}$H$_8$N$_2$ (*M* =180.20 g/mol): orthorhombic, space group *Fddd* (no. 70), *a* = 9.5534(10) Å, *b* = 12.6764(13) Å, *c* = 15.8145(17) Å, *V* = 1915.2(3) Å^3, *Z* = 8, *T* = 173.15 K, µ(MoKα) = 0.076 mm^{-1}, *Dcalc* = 1.250 g/cm^3, 6353 reflections measured (5.928° ≤ 2Θ ≤ 54.642°), 542 unique (R_{int} = 0.0191, R$_{sigma}$ = 0.0082) which were used in all calculations. The final R_1 was 0.0360 (I > 2σ(I)) and wR_2 was 0.1128 (all data). The crystal structure of compound **1** was analyzed using Mercury software [40] versions 3.1 and 4.0.0 and CrystalExplorer 17.5 [41]. The full crystal data have been deposited with the Cambridge Structural Database under CCDC 1971473.

3. Results and discussion

3.1. ^{1}H NMR spectroscopy

A deuterated chloroform sample solution of compound **1** was studied by ^{1}H NMR spectroscopy. Significant changes in chemical shifts were observed in compound **1** (para-substituted pyridine) compared to pyridine and some of its derivatives. For example, the δ 8.63 and 7.41 ppm observed for it in CDCl$_3$ for the ortho and meta protons respectively had shifted via shielding effect to the range of δ 8.60-8.62 ppm and δ 7.28-7.29 ppm for pyridine in the same solvent [42,43]. In 1,4-*bis*(4-pyridyl)butadiyne, the ortho and meta protons are shielded by the diacetylene units, thus resonating at even lower chemical shifts of δ 8.45 and 7.25 ppm [44]. In all, these reported data depict that the effect of substituents on the chemical shifts compared to pyridine and other pyridyl-containing compounds are substantial but not unusual.

3.2. Solid-state structure description

Crystals of compound **1** suitable for X-ray diffraction experiment were grown by slow cooling and evaporation from heptane. It crystallizes orthorhombically in the *Fddd* space group just like **1b** [21]. This runs as an alignment of three perpendicular regular 2-fold axes with one axis running through the central triple bond and the pyridyl N atoms, the second and third run perpendicularly to the first and to each other but above and below the plane of the molecule (Table 1, Figure 2a). With eight (8) molecules per unit cell, it sits on a special position with 222 site symmetry fitting the unique one-quarter of the molecule into the asymmetric unit. Despite being isomorphous, single crystals of **1** and **1b** were grown by slow cooling and evaporation from high boiling non-polar heptane and toluene, respectively. Also, their crystal data were collected at 173 and 100 K, respectively. It is rare to have such a large disparity in the displacement ellipsoids relative to change in temperature from 173 to 100 K while collecting crystal data. Hence the improved **1b** is the reflection of very weak localization of free *bis*(4-pyridyl)acetylene in its lattice.

1a [20] on the other hand crystallizes in the monoclinic space group C2/*m* and possesses parallel and mirror planes that run through the ring side and the triple bond via the two pyridyl nitrogen atoms. These planes are perpendicular to the 2-fold screw and proper rotation axes whose inversion points are located on the mirror planes. It has two molecules per unit cell fitting one-quarter of the molecule into the asymmetric unit (Figure 2b). Its crystal data were collected at a temperature of 133 K, somewhat intermediate between 173 and 100 K.

The pyridyl rings in structure **1** are twisted out of their planes forming a dihedral angle of 51.86° in comparison to those of **1a** which are planar with zero dihedral angle (Figure 3a, 3b). Pyridyl ring twists are experienced by **1**-containing structures (Table 2) **2** [45], **3** [46], **4** [47], **10** [25], **16** [46], **32** [23], **33** [47], **34-39** [52], **40** [53] and **1b** [21] (Figure 4).

Table 1. Geometric parameters for compound **1**.

Atoms	Lengths [Å]	Atoms	Angles [°]	Atoms	Torsions [°]
N(1)-C(1)	1.3298(14)	C(1)-N(1)-C(1)¹	116.30(13)	C(1)-N(1)-C(1)¹-C(2)¹	0.34(8)
C(1)-C(2)	1.3819(16)	N(1)-C(1)-C(2)	124.30(11)	N(1)-C(1)-C(2)-C(3)	-0.66(15)
C(1)-H(1)	0.9500	N(1)-C(1)-H(1)	117.9	C(1)-C(2)-C(3)-C(2)¹	0.30(7)
C(2)-C(3)	1.3885(14)	C(2)-C(1)-H(1)	117.9	C(1)-C(2)-C(3)-C(4)	-179.70(7)
C(2)-H(2)	0.9500	C(1)-C(2)-C(3)	118.68(10)		
C(3)-C(4)	1.438(2)	C(1)-C(2)-H(2)	120.7		
C(4)-C(4)²	1.189(3)	C(3)-C(2)-H(2)	120.7		
		C(2)-C(3)-C(2)¹	117.74(13)		
		C(2)-C(3)-C(4)	121.13(7)		
		C(3)-C(4)-C(4)²	180.0		

Symmetry codes: (1) -x+1/4, -y+1/4, z; (2) x, -y+1/4, -z+5/4.
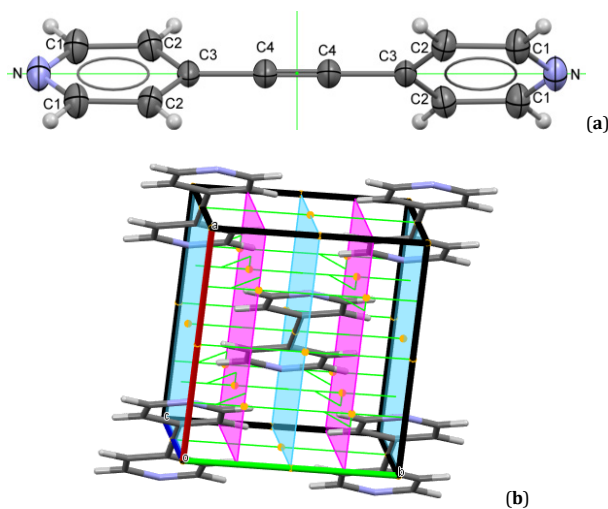
Figure 2. Alignments of the symmetry elements in **1** (**a**) and **1a** (**b**) with symmetry components: Mirror planes (light blue), Glide planes (purple), 2-fold and proper rotation axes (green), Inversion centers (yellow).
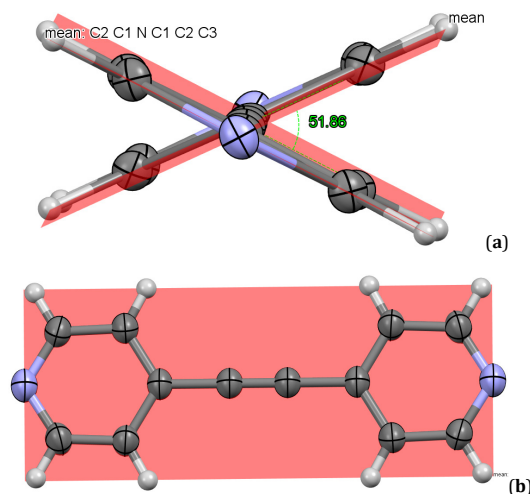

Figure 3. Dihedral angles of the two pyridyl planes in **1** (**a**) and **1a** (**b**).

Compounds **32** (which contains both free and coordinated molecules of compound **1** in the presence of nitrate anions) and **3** (which contains free molecules of **1** in the presence of coordinative ligands and ethanol solvates) experienced greater planar twist of ~79 and 66.67° while others were very low except for **32**'s 51.66°, **40**'s 51.31° and **1b**'s 48.12 °which were somewhat close to **1**'s 51.86°. These structures were considered regardless of their levels of disorder. Thirty-two other structures resemble **1a** with zero dihedral angles (Table 2). The twist in **1** and linearity of the plane in **1a** can be accounted for from their fundamental Wyckoff sites and the molecular symmetries affiliated to them. In **1** in Wyckoff position 8a with site symmetry 222, linearity is imposed on

the N_{pyr}-C_{exo}-C≡C-C_{exo}-N_{pyr} plane with allowance for the heterocyclic pyridine rings to twist about that same plane by the same amount. On the contrary, **1a** possesses a molecular site symmetry of 2/m in the Wyckoff site position 2c. This does result in the alignment of the pyridine rings perpendicularly to the mirror plane which contains the C_{exo}-C≡C-C_{exo} axis thus permitting no allowance for the pyridine rings to twist. The out-of-plane twists in the structure of **1** and its ten (10) counterparts could also be attributed to the level of unsymmetrical tilt experienced by the pyridyl rings as well as a phenomenon associated with the degree of conformational mobility in the molecule.

Table 2. Compilation of bond lengths, bond angles and dihedral angles in co-crystals and metal complexes of compound **1**. Values are calculated at the 99 % confidence level.

REFCODE	C-C (Å)	C≡C (Å)	∠C-N-C (°)	Dihedral (°)	Site symmetry
1a. OLOTUG [20]	1.439*	1.199*	116.3*	0.00	2/m†
1b. OLOTUG03 [21]	1.444*	1.192*	116.9*	48.12	222†
2. QETMUY [45]	1.428 (3) [1.44-1.42]	1.195 (3) [1.20-1.19]	116.5 (2) [117.0-116.0]	7.11	1̄
	1.434 (3) [1.44-1.43]		116.6 (2) [117.1-116.1]		
3. FOTKEG [46]	1.431 (3) [1.44-1.42]	1.197 (3) [1.20-1.19]	117.3 (2) [117.8-116.8]	29.91	2/m
	1.433 (3) [1.44-1.43]		117.3 (2) [117.8-116.8]		
	1.435 (3) [1.44-1.43]	1.197 (3) [1.20-1.19]	116.9 (3) [117.7-116.1]	24.39	2/m
	1.434 (3) [1.44-1.43]		117.2 (2) [117.7-116.7]		
	1.435 (3) [1.44-1.43]	1.202 (3) [1.21-1.19]	117.1 (2) [117.6-116.6]	66.67	2/m
	1.431 (3) [1.44-1.42]		117.2 (3) [118.0-116.4]		
	1.429 (3) [1.44-1.42]	1.200 (3) [1.21-1.19]	117.4 (2) [118.0-116.9]	17.28	2/m
	1.432 (3) [1.44-1.42]		117.4 (2) [118.0-116.9]		
4. LOTFEH [47]	1.436 (4) [1.45-1.43]	1.195 (3) [1.21-1.18]	117.5 (2) [118.0-117.0]	32.80	mm2
	1.439 (4) [1.45-1.43]		118.2 (2) [118.7-117.7]		
	1.442 (4) [1.45-1.43]	1.194 (4) [1.20-1.18]	117.2 (2) [117.7-116.7]	41.68	mm2
	1.438 (4) [1.45-1.43]		117.0 (3) [117.8-116.2]		
5. CAHLON [34]	1.435 (3) [1.45-1.43]	1.187 (3) [1.19-1.18]	117.46*	0.00	2/m
	1.435 (3) [1.45-1.43]		117.5 (3) [118.3-116.7]		
6. RUXMED [24]	1.4366*	1.192*	116.02*	0.00	1̄
	1.437 (2) [1.44-1.43]		116.0 (2) [116.5-115.5]		
7. SUXVUC [48]	1.429 (8) [1.45-1.41]	1.198*	118.1 (6) [119.6-116.6]	0.00	2/m
	1.4292*		118.08*		
8. TACZII [22]	1.434 (3) [1.44-1.43]	1.198*	116.0 (2) [116.5-115.5]	0.00	2/m
	1.4343*		116.05*		
9. TICROO [36]	1.436 (3) [1.44-1.43]	1.187*	115.9 (2) [116.4-115.4]	0.00	1̄
	1.4357*		115.93*		
10. VERKUZ [25]	1.429 (7) [1.45-1.41]	1.191 (8) [1.21-1.17]	116.3 (5) [117.6-115.0]	14.41	2/m
	1.436 (7) [1.45-1.42]		116.5 (5) [117.8-115.2]		
11. XISFEN [49]	1.445 (4) [1.46-1.43]	1.174 (5) [1.19-1.16]	116.5 (3) [117.3-115.7]	0.00	1̄
12. AQOTIK [26]	1.45*	1.16*	120*	0.00	224
13. FOJGOC [50]	1.432 (3) [1.44-1.42]	1.195 (3) [1.20-1.19]	116.3 (2) [116.8-115.8]	0.00	1̄
14. FOTJEF [46]	1.438 (3) [1.45-1.43]	1.197 (3) [1.20-1.19]	116.9 (2) [117.4-116.4]	0.00	2/m
15. FOTJIJ [46]	1.435 (3) [1.44-1.43]	1.197 (3) [1.20-1.19]	117.4 (2) [117.9-116.9]	0.00	2/m
	1.439 (3) [1.45-1.43]		117.2 (2) [117.7-116.7]		
16. FOTKIK [46]	1.427 (4) [1.44-1.42]	1.199 (4) [1.21-1.19]	117.2 (2) [117.7-116.7]	12.70	1̄
	1.427 (4) [1.44-1.42]		116.6 (2) [117.1-116.1]		
	1.425 (4) [1.43-1.42]	1.200 (4) [1.21-1.19]	117.6 (2) [118.1-117.1]	20.55	1̄
	1.428 (4) [1.44-1.42]		116.6 (2) [117.1-116.1]		
17. GIKQEZ [51]	1.435 (2) [1.44-1.43]	1.193 (2) [1.20-1.19]	116.5 (2) [117.0-116.0]	0.00	2/m
18. GIKQEZ01 [51]	1.432 (2) [1.44-1.43]	1.196 (2) [1.20-1.19]	116.3 (2) [116.8-115.8]	0.00	2/m
19. GIKQEZ02 [51]	1.438 (2) [1.44-1.43]	1.190 (2) [1.20-1.18]	116.3 (2) [116.8-115.9]	0.00	2/m
20. GIKQEZ03 [51]	1.436 (3) [1.44-1.43]	1.189 (3) [1.20-1.18]	116.3 (2) [116.8-115.9]	0.00	2/m
21. GIKQEZ04 [51]	1.435 (3) [1.44-1.43]	1.190 (3) [1.20-1.18]	116.6 (2) [117.1-116.1]	0.00	2/m
22. GIKREA [51]	1.426*	1.207*	117.6*	0.00	222
23. GIKREA01 [51]	1.437*	1.189*	117.7*	0.00	222
24. GIKREA02 [51]	1.436*	1.188*	117.8*	0.00	222
25. GIKREA03 [51]	1.435*	1.186*	117.4*	0.00	222
26. GIKREA04 [51]	1.440*	1.182*	117.6*	0.00	222
27. GIKSEB [51]	1.436 (8) [1.46-1.42]	1.180 (8) [1.20-1.16]	115.9 (4) [116.9-114.9]	0.00	1̄
	1.430 (8) [1.45-1.41]	1.199 (8) [1.22-1.18]	116.6 (4) [117.6-115.6]	0.00	
28. GIKSEB01 [51]	1.433 (8) [1.45-1.41]	1.194 (8) [1.21-1.17]	116.3 (5) [117.6-115.0]	0.00	1̄
	1.442 (8) [1.46-1.42]	1.183 (8) [1.20-1.16]	115.4 (5) [116.7-114.1]	0.00	
29. GIKSEB02 [51]	1.436 (8) [1.46-1.42]	1.189 (8) [1.21-1.17]	115.1 (5) [116.4-113.8]	0.00	1̄
	1.426 (8) [1.45-1.41]	1.193 (8) [1.21-1.17]	116.6 (5) [117.9-115.3]	0.00	
30. GIKSEB03 [51]	1.436 (4) [1.45-1.43]	1.183 (4) [1.19-1.17]	115.8 (3) [116.6-115.0]	0.00	1̄
	1.440 (5) [1.45-1.43]	1.181 (5) [1.19-1.17]	115.9 (3) [116.7-115.1]	0.00	
31. GIKSEB04 [51]	1.439 (5) [1.45-1.43]	1.184 (5) [1.20-1.17]	116.1 (3) [116.9-115.3]	0.00	1̄
	1.436 (5) [1.45-1.42]	1.179 (4) [1.19-1.17]	115.4 (3) [116.2-114.6]	0.00	
32. JITQEI [23]	1.45 (2) [1.50-1.40]	1.16 (2) [1.21-1.11]	117 (1) [118-116]	51.66	223
			117 (2) [119-115]		
	1.43*	1.15*	117*	78.98	223
	1.48*		120*		
	1.42 (3) [1.50-1.34]	1.19 (3)	117 (1) [118-116]	79.00	223
	1.45 (3) [1.53-1.37]	[1.27-1.11]	117 (1) [118-116]		
	1.43 (3) [1.51-1.35]	1.22 (3) [1.30-1.14]	117 (1) [118-116]	0.00	223
			118 (1) [119-117]		
	1.45 (3) [1.53-1.37]	1.17 (3) [1.25-1.09]	119 (2) [121-117]	41.86	223
33. LOTFAD [47]	1.436 (3) [1.44-1.43]	1.200 (3) [1.21-1.19]	117.0 (2) [117.5-116.5]	12.99	2/m
	1.434 (3) [1.44-1.43]				
34. MESXOA [52]	1.432 (2) [1.44-1.43]	1.194 (2) [1.20-1.19]	117 (1) [118-116]	9.13	1̄
	1.433 (2) [1.44-1.43]		116.9 (1) [117.2-116.6]		
35. MESXOA01 [52]	1.434 (2) [1.44-1.43]	1.191 (2) [1.20-1.19]	117 (1) [118-116]	9.03	1̄
	1.433 (2) [1.44-1.43]		116.8 (1) [117.1-116.5]		
36. MESXOA02 [52]	1.435 (2) [1.44-1.43]	1.193 (2) [1.20-1.19]	116.7 (1) [117.0-116.4]	8.91	1̄
	1.435 (2) [1.44-1.43]				
37. MESXOA03 [52]	1.434 (2) [1.44-1.43]	1.190 (2) [1.20-1.18]	116.6 (1) [116.9-116.3]	8.75	1̄
	1.435 (2) [1.44-1.43]		116.5 (1) [116.8-116.2]		
38. MESXOA04 [52]	1.432 (3) [1.44-1.42]	1.189 (3) [1.20-1.18]	116.8 (2) [117.3-116.3]	8.62	1̄
	1.433 (2) [1.44-1.43]		116.7 (1) [117.0-116.4]		

Table 2. Continued.

REFCODE	C-C (Å)	C≡C (Å)	∠C-N-C (°)	Dihedral (°)	Site symmetry
39. MESXOA05 [52]	1.432 (3) [1.44-1.42] 1.433 (2) [1.44-1.43]	1.190 (3) [1.20-1.18]	116.8 (1) [117.1-116.5] 116.7 (2) [117.2-116.2]	8.50	1̄
40. MUYLID [53]	1.445* 1.442*	1.179*	117.1	51.31	2/m
41. ROTHIT [54]	1.432 (3) [1.44-1.43]	1.194 (4) [1.20-1.18]	115.9 (2) [116.4-115.4]	0.00	2/m

* Crystallographic values without standard deviations.
† The only two species that formed C-H·····N interactions. H···A = 2.707 Å for OLOTUG and H···A = 2.474 Å for OLOTUG03.
Mean and standard deviation of lengths and angles of structures with dihedral angles > 0: C-C = 1.45 (3)-1.42 (2) Å, C≡C = 1.21 (3)-1.17 (3) Å and ∠C-N-C = 117.7 (8)-116.4 (6)°.
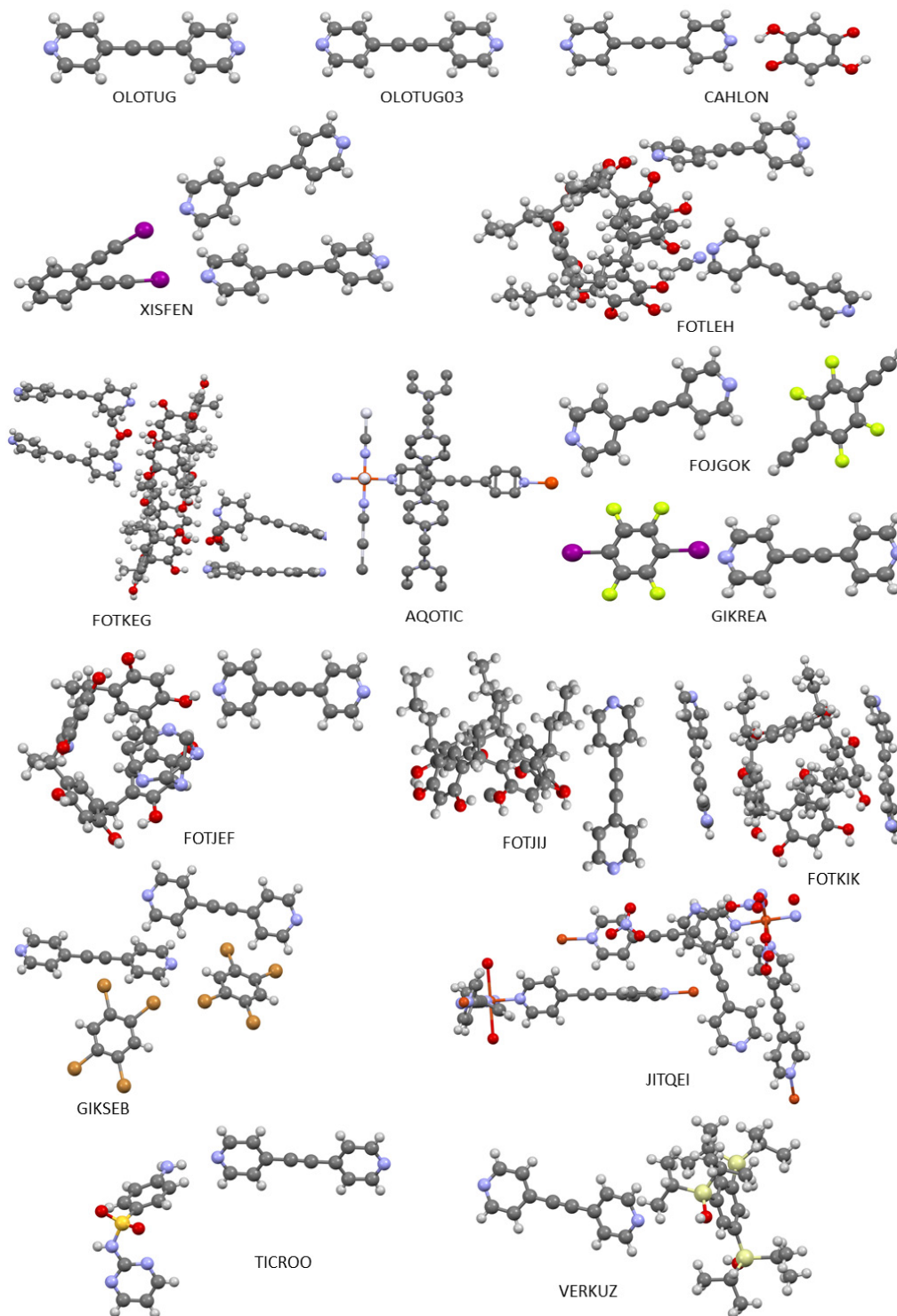

Figure 4. Co-crystals and metal complexes containing compound **1** (Solvates have been omitted for clarity).
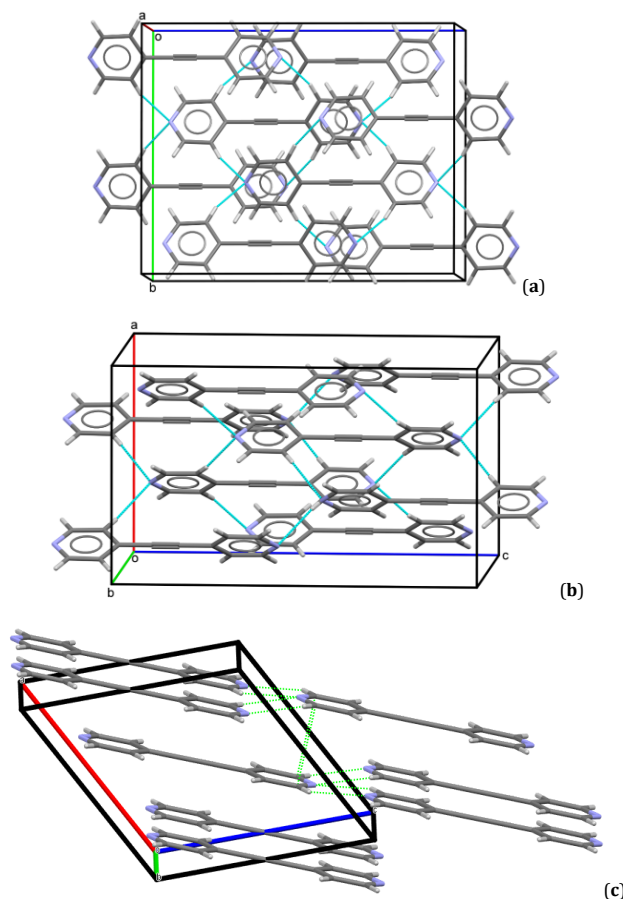
Figure 5. Packing motifs of structures **1** (**a**, **b**) and **1a** (**c**) showing the 2D array of repeated dimeric pairs antiparallel-displaced monomeric units (**a**) connected by edge-to-edge $_{pyr}$C-H·····N$_{pyr}$ supramolecular synthons (**b**) and the close to planar layers formed from corrugated ribbons of intermolecular interactions (**c**) revealing the close proximity of monomeric units necessary for the interaction of non-attractive atoms such as H and C$_\pi$ of the pyridyl periphery.

The dihedral angle of **1** lies close to the median of the all the compound **1** spacers (66.67°) [46] and (41.68°) [47] in two hydrogen-bonded supramolecular frameworks which show the structure of **1** to replicate a similar but rare tilting phenomenon compared to the co-crystals while co-planarity between the pyridyl rings in **1** and its co-crystal-containing molecules are inconsistent. Remarkably, these tilts necessitate the attainment of a close-packed arrangement that is expected to be energetically and sterically optimized as well as having modulational flexibility (Figure 5, Table 2). The centroid-centroid distances of the antiparallel-displaced monomers are 4.327 and 3.684 Å in **1** and **1b**, respectively. Moreover, none of the *bis*(4-pyridyl)acetylene in co-crystals and metal complexes reported in literature was able to self-assemble via C$_{pyr}$-H···N$_{pyr}$ hydrogen bond interactions (Table 2). An obvious reason for this occurrence is that the C$_{pyr}$-H···N$_{pyr}$ hydrogen bond interacttions in structures **1** and **1a** are formed in the absence of Lewis acid/base interaction due to the high purity of the polymorphs. Therefore, they can bind only weakly with each other producing contacts with varying strengths and number. The co-crystals and metal complexes on the contrary have a very strong ability to form short contacts between the pyridyl N donor and a wide list of acceptors. These make the major intermolecular contacts in them to be hetero-molecular in nature thus highlighting the clue to the favored formation of quite a number of these species long before the crystal structures of **1a** and **1b** were reported.

In structure **1**, the exocyclic C-C bond lengths of 1.438 (2) Å and the bond angles of 116.3 (1)° at the pyridyl nitrogen atoms closely agree with those of structure **1a** as well as being symmetrical about the 1,2-positions of the acetylene spacer. Structure **1** possesses a C≡C bond of length 1.189 (2) Å while **1a**'s 1.199 Å is longer. The length of the exocyclic C-C bond is in good agreement with those of diarylalkynes [55]. The trio of the exocyclic C-C (1.4379 (2) Å), C≡C (1.1890 (1) Å) bonds and the bond angle at the pyridyl nitrogen (116.30°) in structure **1** all statistically fall within experimental uncertainty based on 99 % confidence level for twenty-one structures with dihedral angles greater than zero (1.45 (3)-1.42 (2) Å, 1.21 (3)-1.17 (3) Å and 117.7 (8)-116.4 (6)°, respectively) (Table 2). The bond angle of 116.3 (1)° at the pyridyl nitrogen is typical of unprotonated/unmethylated pyridine N and possibly that of **1a**. Structures **1** and **1a** share very close exocyclic C-C bond lengths (1.4379 (2) and 1.439 (3) Å) and CNC bond angles of 116.30°.

The packing motifs of **1** from conventional visualization (Figure 5a, 5b) reveal a 2D arrangement portraying repeated dimeric pairs containing antiparallel-displaced monomeric units wherein each dimeric pair in the 2D array is connected by edge-to-edge "C$_{meta}$-H···N$_{pyr}$" supramolecular synthons: D···A = 3.378 (1) Å; H···A = 2.4722 (7) Å; D-H···A = 159.42 (7)° and a periodic face-to-face stacking that is predictive of π···π interactions in space. **1a** on the other hand forms slightly planar layers formed from grooved ribbon via hydrogen bond interactions. (Figure 5c) The interlayer distance of 3.399 Å falls within the range of interplanar distances of 3.3-3.6 Å established and reported for π···π interactions in planar rings especially pyridine and other aromatic ring containing systems [56].
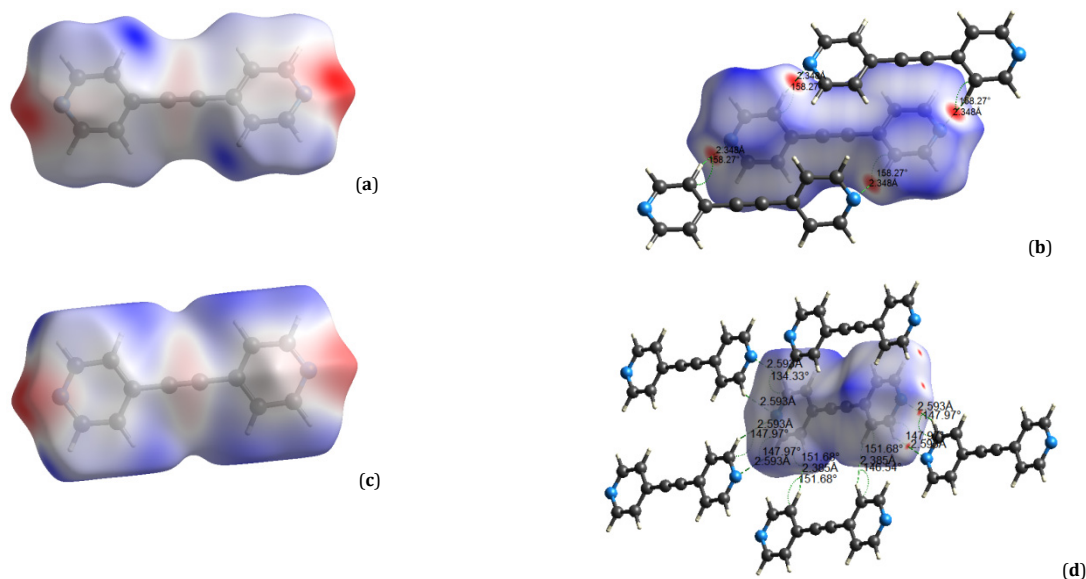
**Figure 6.** The Hirshfeld surface of **1** and **1a** mapped on (**a**) an ESP surface (**a**, **c**) showing the negative and positive ESP regions indicative of proton acceptor and donor potentials, respectively (**b**) d_{norm} (**b**, **d**) showing four red hotspots identifying $C_{pyr\text{-}meta}$-H···N_{pyr} contacts in **1** and eight symmetrically distributed red hotspots attributed to $C_{pyr\text{-}ortho}$-H···N_{pyr} HBIs that are shorter than the summation of the van der Waals radii of nearest neighbor atoms.

The C-H$_{ortho}$···N_{pyr} hydrogen bond interactions (HBIs) in **1a** has values of D···A = 3.558 Å; H···A = 2.707 Å; D-H···A = 149.5°. This HBI is slightly weaker than that for **1** which pinpoints the positive effect of the ring twists in **1**'s pyridine in favouring shorter C_{meta}-H···N_{pyr} in the supramolecular assembly. The H···A values of **1**, **1a** and **1b**'s C_{pyr}-H···N_{pyr} on a general scale are shorter than the sum of the van der Waals radii of 2.75 Å [57,58]. On the other hand, structure **1**'s is shorter than those of co-crystals of acetylene with aromatic azacycles (2.554-2.66 Å) [59] but slightly longer than 2.43 Å (limit of experimental error based on the 99% confidence level) reported for polar assemblies of 2,6-diethynylpyridine.[60] The ∠C_{pyr}-H···N_{pyr} of 159.42 (7)° is higher than **1a**'s 149.5° as well as 147.41° reported for 1,4-*bis*(4-pyridyl)butadiyne whose lower value could be attributed to extensive conjugation [44]. The D-H···A for **1** lies within the range 159 ≥ θ ≤ 180° relative to reports of Okhita and co-workers and Kirchner and co-workers [59,60].

The Hirshfeld surface (HS) of **1** mapped over a 3D electrostatic potential (ESP) surface (Figure 6a) at the Tonto-sourced B3LYP/cc-pVTZ level of theory in the range -0.0669 au (red) through 0.0 (white) to 0.0632 au (blue) showed that the intense red, negative ESP regions indicative of hydrogen acceptors are located on the pyridyl N while another less intense red ESP region hovers over the C≡C bond; reflecting the presence of π electrons. These features are also present in the ESP surface of **1b** at the same level of theory but in the range -0.0722 to 0.0418 au. Intense blue, positive ESP regions indicative of hydrogen donors are located on the meta- and ortho-hydrogen atoms for **1** and **1a**, respectively thus corroborating the earlier information on C_{meta}-H···N_{pyr} and C_{ortho}-H···N_{pyr} HBIs (Figure 6c).

Structure **1**'s HS colored by d_{norm} (Figure 6b) reveals four red hotspots that are shorter than the summation of the van der Waals radii of nearest neighboring atoms. Two are located over the pyridyl N and the other two over the meta C-H bonds of the rings. By generating external fragments, four $C_{pyr\text{-}meta}$-H···N_{pyr} hydrogen bond interactions with $d_{H···N}$ = 2.348 Å and ∠C-H$_{pyr\text{-}meta}$···N_{pyr} = 158.27° were identified. While the conventional visualization via Mercury viewer caught only the $C_{pyr\text{-}meta}$-H···N_{pyr} hydrogen bond interactions, Hirshfeld via d_{norm} surfaces was able to identify and quantify $C_{pyr\text{-}meta}$-H···H-$C_{pyr\text{-}ortho}$ ($d_{H···H}$= 2.883 Å, ∠$C_{pyr\text{-}meta}$-H···H = 122.48°, ∠$C_{pyr\text{-}ortho}$-H···H =

77.48°, ∠$C_{pyr\text{-}meta}$-H···H = 113.06°, ∠$C_{pyr\text{-}ortho}$-H···H= 85.57°, ∠$C_{pyr\text{-}meta}$-H···H= 122.48°, ∠$C_{pyr\text{-}ortho}$-H···H= 85.57°), $C_{pyr\text{-}meta}$-H···C_π ($d_{H···C\pi}$= 2.851 Å, ∠$C_{pyr\text{-}meta}$-H···C_π = 131.65°) C_π···C_π and C_π···N contacts. These corroborate the contacts H···H, H···C_π, C_π···C_π, C_π···N and H···N which had reciprocal contacts occupying surface areas of 41.0, 22.7, 14.5, 0.3 and 21.5%, respectively.

Figure 6d is the HS of structure **1a** coloured by d_{norm} and it reveals eight hotspots that are symmetrically distributed over the pyridyl ends forming $C_{pyr\text{-}ortho}$-H···N_{pyr} HBIs with $d_{H···N}$ = 2.593 Å and ∠$C_{pyr\text{-}ortho}$-H···N_{pyr} = 134.33-147.97 °. The $d_{H···N}$ of **1a** are longer and weaker than those of **1** and the bond angles of the latter are closer to linearity than those of the former. Aside the HBIs identified by the conventional Mercury viewer, Hirshfeld via d_{norm} mappings identified and quantified $C_{pyr\text{-}meta}$-H···H-$C_{pyr\text{-}meta}$ ($d_{H···H}$ = 2.385 Å, ∠$C_{pyr\text{-}meta}$-H···H = 151.68 °, ∠$C_{pyr\text{-}meta}$-H···H = 146.54 °. These are in alignment with N···H and H···H contacts with reciprocal surface areas of 16.9 and 36.9 %. Other contacts such as N···N, C···N, C···H and C···C are present with reciprocal surface areas of 0.3, 3.6, 36.3 and 5.9%. Based on the foregoing, CrystalExplorer has shown the excellent advantage it has over the conventional structure viewer application in unraveling indistinct atom···atom interactions.

This work projects structures **1** and **1a** as containing a pyridine moiety with a strong tendency to self-assemble laterally to form 1D and 2D layers via edge-to-edge C_{pyr}-H···N_{pyr} and edge-to-face $C_{pyr\text{-}meta}$-H···π interactions while the face-to-face π···π stacking between the layers result in a stable 3D network. This is the order of crystal lattices with pyridyl aromatic scaffolds decorated with complementary donor (D = $C_{aromatic}$-H) and acceptor (A = $N_{pyridyl}$) motifs. It was noticed that both conventional and Hirshfeld analyses showed **1** to have shorter and stronger H···N_{pyr} bonds than **1a** by 0.2 Å. One factor that could be responsible for this is the advantage offered by the twist in **1**. The non-covalent attractive forces between D and A bring individual **1** and **1a** monomers in each layer to closer proximity resulting in much closer distances between non-attractive hydrogen atoms (~40-41% H···H), non-attractive hydrogen atoms and carbon atoms (~23-36% H···C_π) and between aromatic carbon atoms (~10-15% C_π···C_π) on the pyridyl periphery (Figures 5 and 6).
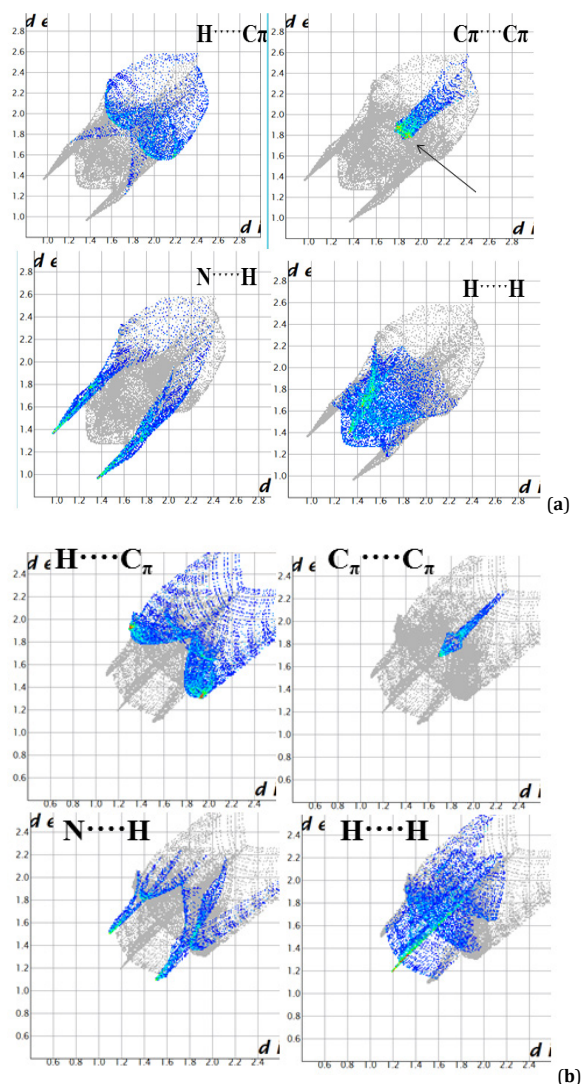
Figure 7. (i) H···C$_\pi$: wings on FPs, (ii) C$_\pi$···C$_\pi$: hot points distributed in d$_i$-d$_e$ region of FPs, (iii) N···H: wings located between spikes and external wings and (iv) H···H: mandibular splitting of the non-bonding contacts located between spikes or antennae for **1** (a) and **1a** (b).

The remarkable rigidity of the acetylene spacer in **1** afforded rigid topologies rather than wavy-layered architectures seen in **1a** and reported for some solid-state investigation of aza-heterocycles [61]. Figure 7 are fingerprint plots (FPs) highlighting the dominating contacts in **1** (Figure 7a) and **1a** (Figure 7b). These plots are simplified 2D representation of complex intermolecular interactions and their information using unique colour plots called fingerprints of those interactions (wings, spikes, mandibular splittings, etc). 2D fingerprint plots herein provide a discernible summary of the number of combinations of external and internal distances (d$_i$ and d$_e$) across the surfaces of **1** and **1a**. So, they do not only show what intermolecular interaction is present, but also the relative area of the surface covered by individual interaction (reciprocal surface area mentioned earlier for diverse contacts).

4. Conclusion

Crystal structures of a number of co-crystals and metal complexes of *bis*(4-pyridyl)acetylene have been reported decades before the valid crystalline reports of pure *bis*(4-pyridyl)acetylene were known. Solid-state studies via conventional and Hirshfeld analytical techniques have proved

to provide valuable answers to these occurrences. The existence of the pure forms of *bis*(4-pyridyl)acetylene are less favorable compared to the co-crystals and metal complexes (metal organic frameworks and the likes); a case of the network stabilities afforded by homo- and hetero-molecular intermolecular contacts respectively.

Acknowledgements

Supporting information Ⓢ

CCDC-1971473 contains the supplementary crystallographic data for this paper. These data can be obtained free of charge via https://www.ccdc.cam.ac.uk/structures/, or by e-mailing data_request@ccdc.cam.ac.uk, or by contacting The Cambridge Crystallographic Data Centre, 12 Union Road, Cambridge CB2 1EZ, UK; fax: +44(0)1223-336033.

Disclosure statement

Conflict of interests: The authors declare that they have no conflict of interest.

Author contributions: René Theodoor Boeré refined the crystal structure model and reviewed the paper; Ibukun Oluwaseun Shotonwa analyzed the data and wrote the main drafts of the paper.

Ethical approval: All ethical guidelines have been adhered.

Sample availability: Samples of the compounds are not available from the author.

ORCID

Ibukun Oluwaseun Shotonwa
http://orcid.org/0000-0002-5364-717X
René Theodoor Boeré
http://orcid.org/0000-0003-1855-360X

References

[1]. Yu, B.; Tracey, J. I.; Cheng, Z.; Vacha, M.; O'Carroll, D. M. *Phys. Chem. Chem. Phys.* **2018**, *20*, 11749-11757.

[2]. Qi, M.; Hulsmann, M.; Godt, A. *J. Org. Chem.* **2016**, *81*, 2549-2571.

[3]. Pearce, T. R.; Waybrant, B.; Kokkoli, E. *Chem. Commun.* **2014**, *50*, 210-212.

[4]. Meineke, D. N. H.; Bossi, M. L.; Ta, H.; Belov, V. N.; Hell, S. W. *Chem. Eur. J.* **2017**, *23*, 2469-2475.

[5]. Liese, S.; Netz, R. R. *Beilstein J. Org. Chem.* **2015**, *11*, 804-816.

[6]. Rupert, B.; Paoli, M. D.; Rupert, B. L.; Mitchell, W. J.; Ferguson, A. J.; Muhammet, E. K.; Rance, W. L.; Rumbles, G.; Ginley, D. S.; Shaheen, S. E.; Kopidakis, N. *J. Mater. Chem.* **2009**, *19*, 5311-5324.

[7]. Cann, J.; Dayneko, S.; Sun, J.; Hendsbee, A. D.; Hill, I. G.; Welch, G. C. *J. Mater. Chem. C* **2017**, *5*, 2074-2083.

[8]. Antina, E. V.; Guseva, G. B.; Loginova, A. E.; Semeikin, A. S.; V'yugin, A. I. *Russ. J. Gen. Chem.* **2010**, *80*, 2374-2381.

[9]. Rajakumar, P.; Visalakshi, K. *Arkivoc*, **2011**, *10*, 213-220.

[10]. Huang, R.; Chiu, Y.; Chang, Y.; Chen, K.; Huang, P.; Chiang, T.; Chang, Y. J. *New J. Chem.* **2017**, *41*, 8016-8025.

[11]. Dallos, T.; Beckmann, D.; Brunklaus, G.; Baumgarten, M. *J. Am. Chem. Soc.* **2011**, *133*, 13898-13901.

[12]. Ni, Z.; Liu, J.; Hoque, M. N.; Liu, W.; Li, J.; Chen, Y.; Tong, M. *Coord. Chem. Rev.* **2017**, *335*, 28-43.

[13]. Fenenko, L.; Shao, G.; Orita, A.; Yahiro, M.; Otera, J.; Svechniko, S.; Adachi, C. *Chem. Commun.* **2007**, 2278-2280.

[14]. Mahmoudpour, A.; Nafisi, S.; Najafi, E.; and Notash, B.; *Main Gr. Met. Chem.* **2019**, *42*, 51-59.

[15]. Faukner, T.; Slany, L.; Sloufova, I.; Vohlidal, J.; Zednik, J. *Macromol. Res.* **2016**, *24*, 441-449.

[16]. Shi, L.; Guo, Y.; Hu, W.; Liu, Y.; *Mater. Chem. Front.* **2017**, *1*, 2423-2456.

[17]. Seth, S.; Matzger, A. J. *Cryst. Growth. Des.* **2017**, *17*, 4043-4048.

[18]. Yuan, S.; Zou, L.; Qin, J.; Li, J.; Huang, L.; Feng, L.; Wang, X.; Bosch, M. *Nat. Commun.* **2017**, *8*, 1-10.

[19]. Yang, X.; Xu, Q. *Cryst. Growth. Des.* **2017**, *17*, 1450-1455.

[20]. Dankhoff, K.; Lochenie, C.; Puchtler, F.; Weber, B. *Eur. J. Inorg. Chem.* **2016**, *2016*, 2136-2143.

[21]. Bajpai, A.; Scott, H. S.; Pham, T.; Chen, K.; Space, B.; Lusi, M.; Perry, M. L.; Zaworotko, M. J. *IUCrJ* **2016**, *3*, 430-439.

[22]. Dias, S. I. G.; S. Rabac, I. C. Santos, D. Wallis, and M. Almeida, *Cryst. Eng. Comm.* **2010**, *12*, 3397-3400.

[23]. Carlucci, L.; Ciani, G.; Macchi, P.; Proserpio, D. M. *Chem. Commun.* **1998**, *1*, 1837-1838.

[24]. Bosch, E. *Cryst. Growth. Des.* **2010**, *10*, 3808-3813, .

[25]. Beckmann, J.; Janicke, S. L. *Eur. J. Inorg. Chem.* **2006**, *2006*, 3351-3358.

[26]. Bartual-murgui, C.; Ortega-Villar, N. A.; Shepherd, H. J.; Munoz, C. M.; Salmon, L.; Bousseksou, A.; Real, J. A. *J. Mater. Chem.* **2011**, *21*, 7217-7222.

[27]. Tsaggeos, K.; Masiera, N.; Niwicka, A.; Dokorou, V.; Siskos, M. G.; Skoulika, S.; Michaelides, A. *Cryst. Growth. Des.* **2012**, *12*, 2187-2194.

[28]. Wang, C.; Batsanov, A. S.; Bryce, M. R.; Martın, S.; Nichols, R. J.; Higgins, S. J.; Suarez, V. M.; Lambert, C. J. *J. Am. Chem. Soc.* **2009**, *131*, 15647-15654.

[29]. Sokolov, A. N.; Tomislav, F.; Blais, S.; Ripmeester, J. A.; Macgillivray, L. R. *Cryst. Growth. Des.* **2006**, *6*, 2427-2428.

[30]. Ryu, J. Y.; Lee, J. M.; Park, Y. J.; Van Nghia, N.; Lee, M. H.; Lee, J. *Organometallics* **2013**, *32*, 7272-7274.

[31]. Neogi, S.; Lorenz, Y.; Engeser, M.; Samanta, D.; Schmittel, M. *Inorg. Chem.* **2013**, *52*, 6975-6984.

[32]. Desiraju, G. R. *J. Am. Chem. Soc.* **2013**, *135*, 9952-9967.

[33]. Choua, S.; Jouaiti, A.; Geoffroy, M. *Phys. Chem. Chem. Phys.* **1999**, *1*, 3557-3560.

[34]. Zaman, B.; Tomura, M.; Yamashita, Y. *J. Org. Chem.* **2001**, *66*, 5987-5995.

[35]. Marin, G.; Andruh, M.; Madalan, A. M.; Blake, A. J.; Wilson, C.; Champness, N. R.; Schroder, M. *Cryst. Growth. Des.* **2008**, *8*, 964-975.

[36]. Elacqua, E.; Bucar, D. -K.; Henry, R. F.; Zhang, G. G. Z.; Macgillivray, L. R. *Cryst. Growth. Des.* **2013**, *13*, 393-403.

[37]. Tanner, M.; Ludi, A. *Chimica* **1980**, *34*, 23-24.

[38]. Sheldrick, G. M. *Acta. Cryst. Sect. A* **2007**, *64*, 112-122.

[39]. Boere, R. T.; Roemmele, T. L.; Yu, X. *Inorg. Chem.* **2011**, *50*, 5123-5136.

[40]. Macrae, C. F.; Bruno, I. J.; Chisholm, J. A.; Edgington, P. R.; McCabe, P.; Pidcock, E.; Rodriguez-Monge, L.; Taylor, R.; Streek, J. V.; Wood, P. A. *J. Appl. Cryst.* **2008**, *41*, 466-470.

[41]. Turner, M. J.; McKinnon, J. J.; Wolff, S. K.; Grimwood, D. J.; Spackman, P. R.; Jayatilaka, D.; Spackman, M. A. CrystalExplorer17, University of Western Australia, 2017.

[42]. BioCIS UMR-CNRS-8076, Universite de Paris-Saclay, France, Retrieved Feb 01, 2020, from https://www.sigmaaldrich.com/nmr

[43]. Fulmer, G. R.; Miller, A. J. M.; Sherden, N. H.; Gottlieb, H. E.; Nudelman, A.; Stoltz, B. M.; Bercaw, J. E.; Goldberg, K. I. *Organometallics* **2010**, *29*, 2176-2179.

[44]. Allan, J. R.; Barrow, M. J.; Beaumont, P. C.; Macindoe, L. A.; Milburn, G. H. W.; Werninck, A. R. *Inorg. Chim. Acta* **1988**, *148*, 85-90.

[45]. Sokolov, A. N.; Friscic, T.; Blais, S.; Ripmeester, J. A.; Macgillivray, L. R. *Cryst. Growth Des.* **2006**, *6*, 2427-2428.

[46]. Patil, R. S.; Mossine, A. V.; Kumari, H.; Barnes, C. L.; Atwood, J. L. *Cryst. Growth Des.* **2014**, *14*, 5212-5218.

[47]. Patil, R. S.; Kumari, H.; Barnes, C. L.; Atwood, J. L. *Chem. Commun.*, **2015**, *51*, 2304-2307.

[48]. Tomura, M.; Yamashita, Y. *Chem. Lett.* **2001**, *6*, 532-533.

[49]. Bosch, E.; Kruse, S. J.; Groeneman, R. H.; *Cryst. Eng. Comm.* **2019**, *21*, 990-993.

[50]. Bosch, E. *J. Chem. Crystallogr.* **2014**, *44*, 287-292.

[51]. Hutchins, K. M.; Unruh, D. K.; Carpenter, D. D.; Groeneman, R. H. *Cryst. Eng. Comm.* **2018**, *20*, 7223-7402.

[52]. Hutchins, K. M.; Unruh, D. K.; Verdu, F. A.; Groeneman, R. H. *Cryst. Growth. Des.* **2018**, *18*, 566-570.

[53]. Bosch, E.; Bowling, N. P.; Darko, J. *Cryst. Growth. Des.* **2015**, *15*, 1634-1641.

[54]. Hutchins, K. M.; Dutta, S.; Loren, B. P.; Macgillivray, L. R. *Chem. Mater.* **2014**, *26*, 3042-3044.

[55]. Allen, F. H.; Kennard, O.; Watson, D. G.; Brammer, L.; Orpen, A. G. *J. Chem. Soc. Perkin Trans. II* **1987**, *12*, S1-S19.

[56]. Mishra, B. K.; Sathyamurthy, N. *J. Phys. Chem. A* **2005**, *109*, 6-8.

[57]. Bondi, A. *J. Phys. Chem.* **1964**, *68*, 441-451.

[58]. Batsanov, S. S. *Inorg. Mater.* **2001**, *37*, 871-885.

[59]. Kirchner, M. T.; Boese, R.; Gehrke, A.; Blaser, D. *Cryst. Eng. Comm.* **2004**, *6*, 360-366.

[60]. Ohkita, M.; Suzuki, T.; Nakatani, K.; Tsuji, T. *Chem. Lett.* **2001**, *30(10)*, 988-989.

[61]. Shivakumar, K.; Vidyasagar, A.; Naidu, A.; Gonnade, R. G. Sureshan, K. M. *Cryst. Eng. Comm.* **2012**, *14*, 519-524.